Hexagonal Sodium Yttrium Fluoride Based Green and Blue Emitting Upconversion Phosphors

Karl W. Krämer,*,† Daniel Biner,† Gabriela Frei,† Hans U. Güdel,† Markus P. Hehlen,‡,§ and Stefan R. Lüthi‡,||

Department of Chemistry and Biochemistry, University of Bern, Switzerland, and Gemfire Corporation, 1220 Page Avenue, Fremont, California 94538

Received September 1, 2003. Revised Manuscript Received January 12, 2004

Hexagonal sodium yttrium fluoride, $NaYF_4$, is the most efficient host material to date for green (Yb^{3+}/Er^{3+} doped) and blue (Yb^{3+}/Tm^{3+} doped) upconversion (UC) phosphors, i.e., phosphors which emit visible light upon infrared (IR) excitation. The structure of the hexagonal phase gives rise to controversy about the cation sites and distribution. The X-ray diffraction patterns of our phosphors do not fit well with the crystal structure reported for $NaNdF_4$ (space group $P\bar{6}$, $Z = 1.5$). The Na:M ratio (M = Y, Nd, Er, Tm, Yb) of the hexagonal phase deviates significantly from 1:1, and it depends on M and the preparation temperature. It is proposed that the hexagonal phase is isostructural to the chlorides $Na_{3x}M_{2-x}Cl_6$ with M = La−Sm. This structure (space group $P6_3/m$, $Z = 1$) contains only one M^{3+} site which is partially occupied by Na^+, and the formula $Na_{3x}M_{2-x}F_6$ ($x \approx 0.45$) accounts for the nonstoichiometry. The model was derived from powder X-ray diffraction on the green and blue phosphor materials as well as the pure Nd, Y, and Yb compounds. The light emission properties of the material crucially depend on the phase purity, doping ratio, Na:M ratio, and preparation temperature. Because earlier spectroscopic investigations generally suffered from impure materials which reduced the UC efficiency, a new, reproducible preparation route was developed. Its key features are an excess of NaF in the synthesis, i.e., a 2:1 ratio of Na:M, the use of HF gas for fluorination, and a process temperature lower than the melting point of the respective NaF/MF_3 eutecticum. It yields the pure hexagonal phase without admixture of the cubic phase or other impurities except for minor inclusions of NaF. Upon IR excitation at 10 245 cm^{-1}, the samples doped with 18% Yb + 2% Er and 25% Yb + 0.3% Tm showed the highest UC efficiencies for green and blue emission, respectively. Relative UC efficiencies were measured with a powder test setup in a standard procedure. The doping ratios and all steps of the synthesis were optimized with respect to the UC efficiency. The obtained phosphor materials show no degradation under high-power IR laser excitation.

Introduction

To our knowledge, hexagonal $NaYF_4$ is the most efficient host material for green and blue UC phosphors, i.e., phosphors which show visible emission upon IR excitation.[1,2] The UC process has attracted considerable interest in the fields of lighting and display technology since the development of IR laser diodes. In the title material, Y^{3+} can be replaced in any ratio by rare-earth ions, e.g., by Yb^{3+} and Er^{3+} or by Yb^{3+} and Tm^{3+} for green or blue UC phosphors, respectively. However, it remains an open question why the UC efficiency in this host material is superior to that of others.

The quasi binary phase diagrams $NaF-MF_3$ with M = Y, La−Lu were studied by Thoma et al.[3] They found incongruently melting hexagonal phases $NaF{\cdot}MF_3$ for all M. A certain phase width is shown in the phase diagrams for M = Y, Nd−Lu for high temperatures but not further discussed. The hexagonal phases of the heavier lanthanides transform to cubic fluorite-type structures above 600−700 °C depending on the M^{3+} size. The crystal structure of the hexagonal phase was determined by Burns[4] for $NaNdF_4$ with lattice parameters of $a = 6.100$ Å, $c = 3.711$ Å, space group $P\bar{6}$, and $Z = 1.5$. Sobolev et al.[5] related the structure of $NaYF_4$ to gagarinite, $NaCaLaF_6$, with space group $P6_3/m$. Both models are variants of the UCl_3 structure.[6] They agree on the position of 6 F^- anions per unit cell, but there are differences about the cation sites and distribution.

* To whom correspondence should be addressed. Phone: +41 31 631 4248. Fax: +41 31 631 4399. E-mail: karl.kraemer@iac.unibe.ch.
† University of Bern.
‡ Gemfire Corporation.
§ Present address: Los Alamos National Laboratory, LANSCE-12, Mailstop H805, Los Alamos, NM 87545.
|| Present address: Dept. of Physics, Univ. Federal de Pernambuco, Recife, Brazil.

(1) Hehlen, M. P.; Philips, M. L. F.; Cockroft, N. J.; Güdel, H. U. In *Encyclopedia of Materials: Science and Technology* (ISBN 0-08-0431526); Burschow, K. H. J., Ed.; Elsevier Science Ltd.: New York, 2001; p 9456.
(2) Phillips, M. L. F.; Hehlen, M. P.; Nguyen, K.; Sheldon, J. M.; Cookroft, N. J. *Proc. Electrochem. Soc.* **2000**, *99−40*, 123.
(3) Thoma, R. E.; Insley, H.; Hebert, G. M. *Inorg. Chem.* **1966**, *5*, 1222.
(4) Burns, J. H. *Inorg. Chem.* **1965**, *4*, 881.
(5) Sobolev, B. P.; Mineev, D. A.; Pashutin, V. P. *Dokl. Akad. Nauk SSSR* **1963**, *150*, 791.
(6) Meyer, G.; Wickleder, M. S. *Handbook of the Physics and Chemistry of Rare Earths*, Vol. 28 (ISBN 0-444-50346-3); Elsevier Science Ltd.: New York, 2000; pp 67 and 72.

10.1021/cm031124o CCC: $27.50
Published on Web 03/02/2004

Other studies tried to derive the cation positions by luminescence spectroscopy from the $^5D_0$ emission of Eu^{3+} in $NaGdF_4$: Ce, Eu,[7] and $NaEuF_4$,[8] but experiments revealed the presence of more transitions than theoretically expected and prevented unambiguous results. The X-ray diffraction patterns of our phosphors do not fit well with the published $NaNdF_4$ structure.[4] It is proposed that the hexagonal phase is isostructural to the chlorides $Na_{3x}M_{2-x}Cl_6$ with M = La−Sm,[9,10] an addition/substitution variation of the UCl_3 type structure.

The UC properties of hexagonal sodium yttrium fluoride based phosphors have previously been examined. Kano et al.[11] determined the green UC efficiency for Yb, Er codoped samples as a function of composition and firing temperature. The optimum conditions were found to be 30−40% Yb, 3−4% Er, and 630 °C. Menyuk et al.[12] investigated a sample with 18% Yb and 2% Er prepared at 1000 °C. A variety of Yb, Er and Yb, Tm codoped commercially available UC phosphors were examined by Page et al.[13] for UC efficiency, and the UC process was modeled as a function of excitation power. Formerly investigated samples generally suffered from impurity phases, e.g. the cubic phase of $NaYF_4$, oxide compounds such as YOF, or binary starting materials which all reduce the UC efficiency. When our work on the Yb, Er and Yb, Tm doped phosphors started, we first established a new preparation route which yields reproducibly the pure hexagonal phase. Several parameters are crucial for the synthesis of this material. Some appeared to be different from previous reports or had not been addressed before. Besides the doping ratio, mainly the phase purity, the Na:M ratio, and the preparation temperature determine the UC efficiency. Those parameters were optimized for green and blue phosphors using optical measurements, powder X-ray diffraction, differential scanning calorimetry, and scanning electron microscopy.

Experimental Section

Synthesis. The phosphor powder samples were prepared from rare-earth oxides M_2O_3 (M = Y, Nd, Er, Tm, Yb) of 5 N or 6 N purity, Na_2CO_3, 47% HBr, and 40% HF acids in H_2O. Batches were typically calculated for 5 g of product. Oxides M_2O_3 were dissolved in a small amount of HBr in a Teflon beaker, evaporated to dryness, dissolved in water, and the fluorides MF_3 precipitated with HF. The liquid was evaporated and HF was added again. An amount of Na_2CO_3 to obtain a 2:1 ratio of Na:M was dissolved in water in a separate beaker and slowly added to the mixture. Care has to be taken to avoid spilling due to the CO_2 evolution. The product was dried, and the addition of HF and drying were repeated. The solid, which consists of a mixture of MF_3, NaF, and NaBr according to X-ray diffraction, was ground up in a mortar, transferred into a glassy carbon boat, and heated to 550 °C in a HF/Ar gas stream for 20 h. In this step, the reaction toward the hexagonal sodium yttrium fluoride phase plus excess NaF took place. Traces of O and Br were removed by the HF gas stream. The powder was ground up again and heated to 590 °C in an Ar gas stream for another 20 h. This step is necessary to obtain a phosphor of highest UC efficiency, as will be discussed below. The HF/heat process utilizes an apparatus for gas handling made from all PFA tubing and valves. The heat-exposed parts are made from Ni 600 alloy which is resistant to HF gas in the applied temperature range. The HF gas, about 5 g per batch, is generated from KHF_2 in a glassy carbon crucible which is heated in an Ar gas stream. Finally, the product was washed with water to dissolve the excess NaF and then dried at 100 °C.

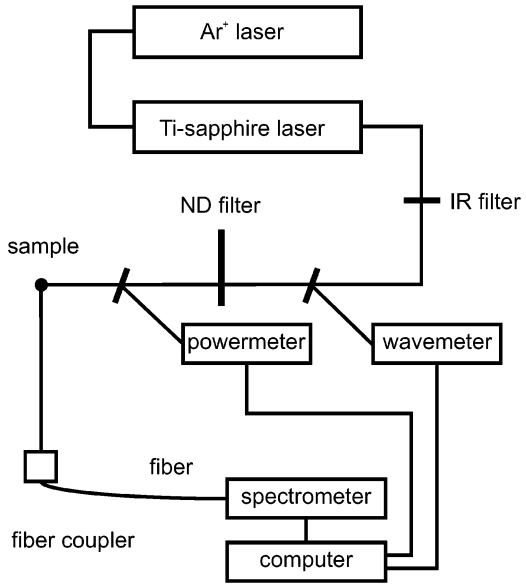

Figure 1. Scheme of the upconversion powder test setup.

X-ray Diffraction. X-ray powder diffraction patterns were measured on a Stoe STADI P diffractometer at room temperature. A Bragg−Brentano reflection geometry was used with α-SiO_2 (101) monochromated Cu $K\alpha_1$ radiation (λ = 1.540598 Å). The diffraction diagrams were recorded with a linear position-sensitive detector in a 2θ range of 10−100° or 150° with a resolution of 0.01°. Data were evaluated with the WinXPow software[14] and structures were refined by the FULLPROF program.[15]

DSC. The phase transitions of the samples were examined by differential scanning calorimetry (DSC) on a Mettler-Toledo DSC 25 system. Samples of 5−10 mg were heated in Al_2O_3 containers at 5 K/minute in a N_2 gas stream.

SEM. Scanning electron microscope (SEM) images were taken on a JEOL JSM 840 to characterize the morphology and size distribution of the phosphor powder grains.

Upconversion Powder Test Setup. An optical setup was developed for the fast and reproducible determination of relative UC efficiencies of the phosphor samples (Figure 1). An Ar^+ laser (Spectra Physics 2045) pumped Ti-sapphire laser (Spectra Physics 3900S) was used as a powerful, tunable IR source. The laser beam passed through a color filter (Schott, RG 830) to cut off visible light, through beam splitters which couple off light for wavelength (Burleigh WA 2500) and power (Coherent Labmaster E) measurements, and through a neutral density filter for power adjustment, before hitting the sample without focusing. The phosphor powders were filled in 1.5-mm-diameter glass tubes and reproducibly positioned in a sample holder. The emitted light was coupled into a fixed optical fiber and measured in the range of 250−500 nm or 500−1000 nm by a spectrometer with a CCD-array detector

(7) Kiliaan, H. S.; Kotte, J. F. A. K.; Blasse, G. *Chem. Phys. Lett.* **1987**, *133*, 425.
(8) Zakaria, D.; Mahiou, R.; Avignant, D.; Zahir, M. *J. Alloys Compd.* **1997**, *257*, 65.
(9) Krämer, K.; Meyer, G. *Z. Anorg. Allg. Chem.* **1990**, *589*, 96.
(10) Lissner, F.; Krämer, K.; Meyer, G.; Hu, Z.; Kaindl, G. *Z. Anorg. Allg. Chem.* **1994**, *620*, 444.
(11) Kano, T.; Yamamoto, H.; Otomo, Y. *J. Electrochem. Soc.* **1972**, *119*, 1561.
(12) Menyuk, N.; Dwight, K.; Pierce, J. W. *Appl. Phys. Lett.* **1972**, *21*, 159.
(13) Page, R. H.; Schaffers, K. I.; Waide, P. A.; Tassano, J. B.; Payne, S. A.; Krupke, W. F.; Bischel, W. K. *J. Opt. Soc. Am. B* **1998**, *15*, 996.
(14) WinXPow software package; STOE & CIE GmbH, Darmstadt, Germany.
(15) Rodriguez-Carvajal, J. *Physica B* **1993**, *192*, 55.

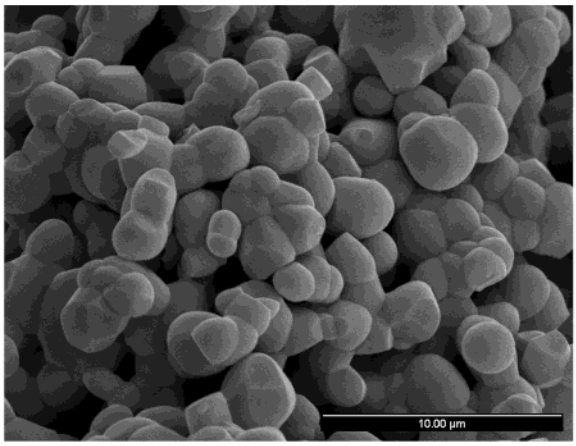

Figure 2. Scanning electron microscope image of a Yb, Er doped green phosphor.

(Ocean Optics SD1000). The spectra were converted to number of photons per cm^{-1}, corrected for the spectral response of the detection system, and the emission bands integrated to yield relative efficiencies. The reproducibility of the setup was ± 1%.

Results and Discussion

Morphology. After the synthesis, the phosphor material consists of a powder that is sintered together. The spherically shaped crystals of 1−3 μm size grow together and form larger aggregates which are partially broken up again in a mortar. The samples are uniform without a visible admixture of any impurity phase. An electron microscope image of a typical sample is shown in Figure 2.

Structure. The crystal structure of the phosphor materials was refined by the Rietveld method from X-ray powder diffraction data (Figure 3). The phosphor materials consist of the hexagonal sodium rare-earth fluoride phase. Some samples contained a small residual amount of NaF (typically 1−3%), most obvious from its 200 reflection at 38.8° 2θ. The NaF content was determined as 0.9(1)% for the X-ray pattern shown in Figure 3. No traces of the cubic phase or any other impurity were detected by X-ray diffraction. In the refinement, a total of 22 parameters were used in a full matrix least-squares fit including the NaF impurity phase. Of those, 9 were profile parameters (1 zero point, 2 scale factors, 3 half width, 2 asymmetry, and 1 shape parameters) and 13 were structural parameters (2 lattice, 2 positional parameters, 1 occupation, and 8 anisotropic temperature factors). The results are summarized in Tables 1 and 2. The crystal structure is shown in Figure 4.

The X-ray pattern was refined using the $Na_{3x}M_{2-x}Cl_6$ structure type with M = La−Sm[9,10] in space group $P6_3/m$. As will be discussed below in detail, this model fits our diffraction data better than the $NaNdF_4$ structure[4] which is the commonly used model for the hexagonal phase. Both are addition/substitution variations of the UCl_3 structure type.[6,10] UCl_3 crystallizes in space group $P6_3/m$ with 2 formula units in the hexagonal unit cell ($Z = 2$). U^{3+} ions on site (2c) are coordinated by 9 Cl^- ions on site (6h) in the shape of a tricapped trigonal prism. The U^{3+} and Cl^- ions are replaced by rare-earth M^{3+} and F^- ions, respectively. In the $Na_{3x}M_{2-x}F_6$ structure M^{3+} is partially substituted by Na^+ on the (2c) site. For each of those, two further Na^+ ions are added on the formerly unoccupied site (2b) for charge compensation. This results in the formula $Na1_{2x}(Na2_xM_{2-x})F_6$ or, abbreviated, $Na_{3x}M_{2-x}F_6$. As expected, there is no indication for an occupation of the (2a) or (4e) sites by Na^+.[6,9,10] The coordination polyhedron of the Na1 site (2b) is a trigonally compressed octahedron. The short

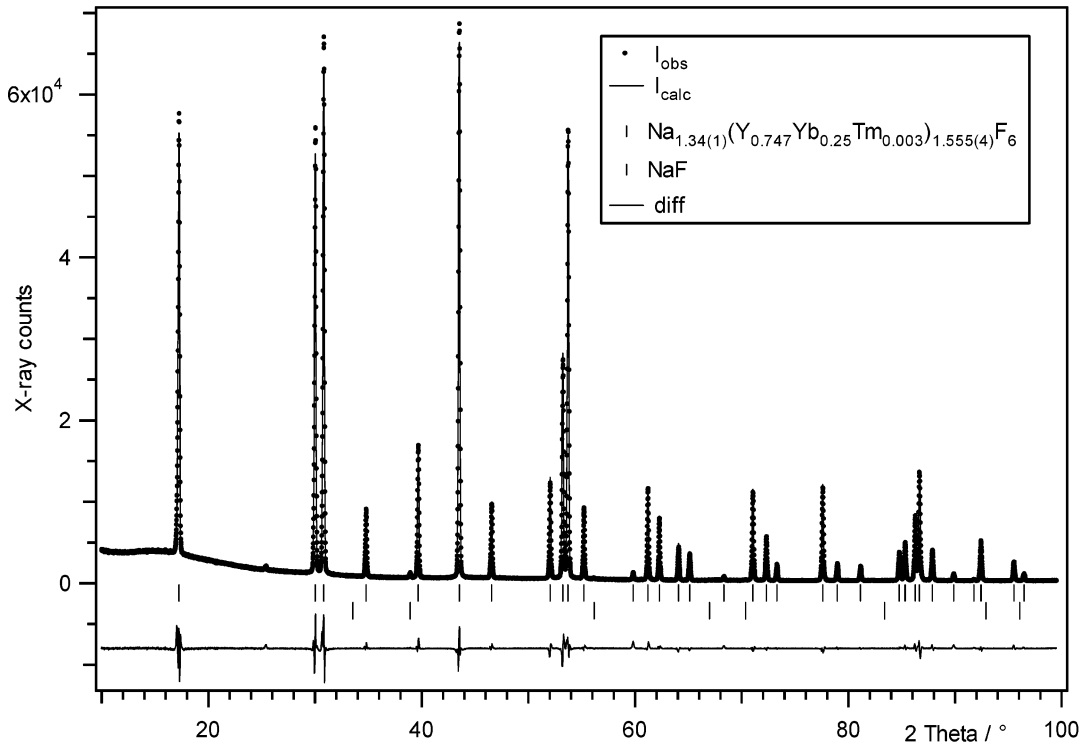

Figure 3. Rietveld fit of a X-ray powder diffraction diagram of hexagonal $Na_{3x}M_{2-x}F_6$ (cf. Table 1, no. 6).

Table 1. Composition, Preparation Temperature, Lattice Parameters, and F *x/a* and *y/b* Positional Parameters ($z/c = 0.25$) of $Na_{3x}M_{2-x}F_6$ Compounds

no.	$Na_{3x}M_{2-x}F_6$	M[a]	*x*	*T*/°C	*a*/Å	*c*/Å	F *x/a*	F *y/b*
1	$Na_{1.40(1)}M_{1.534(4)}F_6$	Nd_{100}	0.466(4)	675	6.1065(1)	3.71794(5)	.3878(4)	.3077(4)
2	$Na_{1.30(1)}M_{1.566(5)}F_6$	Y_{100}	0.434(5)	580	5.97567(5)	3.53053(5)	.3907(2)	.3098(2)
3	$Na_{1.32(3)}M_{1.561(9)}F_6$	Yb_{100}	0.439(9)	555	5.94058(5)	3.48101(5)	.3916(4)	.3113(4)
4	$Na_{1.40(1)}M_{1.534(4)}F_6$	$Yb_{25}Tm_{0.3}$	0.466(4)	550	5.9668(1)	3.51827(5)	.3893(3)	.3084(3)
5	$Na_{1.38(1)}M_{1.539(4)}F_6$	$Yb_{25}Tm_{0.3}$	0.461(4)	580	5.9682(1)	3.51908(5)	.3879(2)	.3082(3)
6	$Na_{1.34(1)}M_{1.555(4)}F_6$	$Yb_{25}Tm_{0.3}$	0.445(4)	600	5.9678(1)	3.51871(5)	.3905(2)	.3092(3)
7	$Na_{1.17(1)}M_{1.610(4)}F_6$	$Yb_{25}Tm_{0.3}$	0.390(4)	620	5.9693(1)	3.5198(1)	.3890(3)	.3090(3)
8	$Na_{1.364(7)}M_{1.545(3)}F_6$	$Yb_{25}Tm_{0.4}$	0.455(2)	590	5.96715(5)	3.51805(5)	.3899(2)	.3089(2)
9	$Na_{1.32(1)}M_{1.558(4)}F_6$	$Yb_{30}Tm_{0.4}$	0.442(4)	590	5.96557(5)	3.51576(5)	.3911(3)	.3095(3)
10	$Na_{1.46(1)}M_{1.514(4)}F_6$	$Yb_{35}Tm_{0.4}$	0.486(4)	590	5.96426(5)	3.51327(5)	.3899(3)	.3089(3)
11	$Na_{1.361(7)}M_{1.546(2)}F_6$	$Yb_{30}Tm_{0.5}$	0.454(3)	590	5.96510(5)	3.51552(5)	.3909(2)	.3098(3)

[a] Doping level in %. The missing fraction to 100% is Y.

Table 2. Positional Parameters, Site Occupation Factors (sof), Temperature Factors, and Atomic Distances of $Na_{1.34(1)}(Y_{0.747}Yb_{0.25}Tm_{0.003})_{1.555(4)}F_6$ (cf. Table 1, no. 6), Space Group $P6_3/m$ [a]

atom	site	*x/a*	*y/b*	z/*c*	sof	U_{11}	U_{22}	U_{33}	U_{12}
Na1	(2b)	0	0	0	.0742(5)	.0047(4)	$= U_{11}$	.219(8)	$= U_{11}/2$
Y	(2c)	1/3	2/3	1/4	.0972(2)	.0059(3)	$= U_{11}$	.0076(2)	$= U_{11}/2$
Yb	(2c)	1/3	2/3	1/4	.03240(6)	.0059(3)	$= U_{11}$	.0076(2)	$= U_{11}/2$
Na2	(2c)	1/3	2/3	1/4	.0371(3)	.0059(3)	$= U_{11}$	.0076(2)	$= U_{11}/2$
F	(6h)	.3905(2)	.3092(3)	1/4	1/2	.022(1)	.009(1)	.008(1)	.009(1)
distances/Å		Y, Yb, Na2 − F			3 * 2.323 6 * 2.365	Na1 − F		6 * 2.304	

[a] $R_p = 4.3\%$, $R_{wp} = 6.6\%$, $R_{Bragg} = 2.1\%$, $\chi^2 = 8.6$. $U_{13} = U_{23} = 0$, $U_{ij}/Å^2$. sof(Y + Yb + Na2) = 1/6, sof(Na1) = 2*sof(Na2). The Tm content on site (2c) was neglected in the X-ray structure refinement.

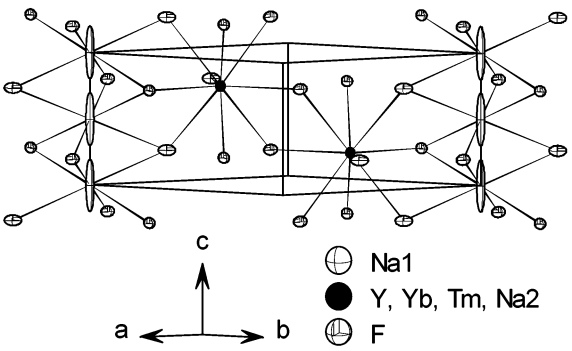

Figure 4. Perspective view along 110 onto the crystal structure of hexagonal $Na_{3x}M_{2-x}F_6$ (cf. Table 2).

distance of $c/2 = 1.76$ Å between neighboring positions along the *c*-axis allows a maximum occupation of only every second position along the *c*-axis (Figure 4). This restriction of $x \leq 1/2$ results in the limiting composition $Na_{1.5}M_{1.5}F_6 = NaMF_4$. The determined Na content *x* was significantly lower than for $x = 1/2$ in all samples under investigation (Table 1).

A closer inspection of the diffraction pattern reveals the presence of weak intensity for the 001 reflection at $2\theta = 25.4°$ (Figure 3). For space group $P6_3/m$ this reflection is symmetry forbidden (00*l* with $l = 2n$ only) at a first glance. Its intensity originates from the partial occupation of site (2b) by Na. These Na1 are not statistically distributed, as discussed above. The actual situation is a $Na_x\square_{1-x}$ chain along the *c*-axis with $x \leq 1/2$ and all Na having neighboring vacancies (□). This results in an alternating Na□ chain for $x = 1/2$; but with decreasing *x* the number of vacancies increase. For the observed range of *x* (Table 1), larger fragments of Na□ chains separated by several vacancies are expected. These chain fragments lower the symmetry and give rise to the intensity of the 001 reflection, a situation which cannot be treated exactly in any space group.

The $NaNdF_4$ structure[4] with space group $P\bar{6}$ and $Z = 1.5$ is the hitherto commonly used model for the hexagonal phase. It has two different sites with 9-fold coordination: one occupied by Nd^{3+} only, and the other occupied by Nd and Na in a 1:1 ratio. A refinement of our data in this model leads to slightly worse *R*-values as for the $Na_{3x}M_{2-x}F_6$ one. But, whereas the $Na_{3x}M_{2-x}F_6$ model even allows a refinement of anisotropic temperature factors, the $NaNdF_4$ model results in negative temperature factors for the mixed Nd/Na site already for an isotropic refinement. This is a clear indication for an incorrect electron density and points toward a mixed Nd/Na occupation for both 9-fold sites. Because the average M−F distances of 2.410 and 2.466 Å[4] for those sites are similar, a partial occupation of only one of them by Na is not intuitive. Second, the Na:M ratio in our compounds significantly deviates from 1:1, as is discussed below in detail. This is not accounted for in the $NaNdF_4$ model. Furthermore, the lower symmetry of space group $P\bar{6}$ results in additional structural parameters: Na1 on 0,0,*z* and a second F site F2 on *x*,*y*,0.5, i.e., 5 parameters instead of 2 as for $P6_3/m$. Because the $P6_3/m$ model yields a better agreement with the data, using a lower number of parameters, and physically meaningful parameter values, we believe it is the most adequate description of the structure.

Recently, Grzechnik et al. reported high-pressure studies on hexagonal $Na_{1.5}Y_{1.5}F_6$.[16] They discussed several structural models and attributed the hexagonal phase to the published $NaNdF_4$ structure[4] up to 20 GPa due to the presence of the 001 reflection. For 1.5 GPa they report Y1−F and (Y2/Na)−F mean distances of 2.485 and 2.142 Å for the 9-fold coordination sites, respectively. Considering the Na^+ ionic radius is significantly larger than that of Y^{3+} (1.24 Å and 1.075 Å

(16) Grzechnik, A.; Bouvier, P.; Mezouar, M.; Mathews, M. D.; Tyagi, A. K.; Köhler, J. *J. Solid State Chem.* **2002**, *165*, 159.

for C. N. 9, respectively),[17] it can hardly be rationalized that (Y2/Na) should occupy the smaller site. Even more striking is the distorted octahedral Na coordination (site (2h) in $P\bar{6}$) with Na−F distances of 2.116 and 2.636 Å (3*x* each). Such different distances cannot be rationalized from a chemical or crystallographic point of view. We attribute these problems to fitting artifacts due to the incorrect structural model.

The hexagonal $Na_{3x}M_{2-x}F_6$ structure is also related to the mineral gagarinite[5] $Na_zCa_zLa_{2-z}F_6$ with $z \leq 1$. Both have the same space group ($P6_3/m$) and atomic sites. The sodium occupation factor of 0.450(5) for site (2b) in $Na_zCa_zY_{2-z}F_6$[18] is very similar to our results in Table 1. Some authors report sodium on the (4e) site 0,0,*z* with $z \approx 0.07$ instead of the (2b) site.[19,20] Our data are most consistent with Na1 on the 0,0,0 position, i.e., the center of the trigonally compressed octahedron. The Na1−F distance of 2.304 Å (Table 2) corresponds very well to that of 2.317 Å in NaF.[21] On the other hand, Na1 shows a huge U_{33} temperature factor in our refinement (Figure 4). This indicates a strong dynamic displacement along the *c*-axis. It might be due to hopping of sodium ions onto unoccupied positions of the (2b) site in the sense of a 1D ionic conductor. Ionic conductivity was recently reported for powder samples of isostructural Cl and Br compounds.[22] The high value of U_{33} is characteristic for this structure type and was also observed in the single-crystal refinements.[9,10,18]

Sodium Content. The sodium content *x* of the hexagonal $Na_{3x}M_{2-x}F_6$ phase was determined from the structure refinement. It varies as a function of the rare-earth (mixture) M and the temperature applied during the synthesis, as shown in Table 1. As a sodium excess was used in the preparation (the Na:M ratio was 2:1), the sample composition stated in Table 1 represents the maximum sodium content which could be incorporated into the structure under the respective conditions. The pure compounds with M = Nd, Y, and Yb (Table 1, nos. 1−3) show a decreasing *x* along the rare-earth series. As expected, the lattice parameters shorten with decreasing M^{3+} ionic radii. The ionic radius of Y^{3+} fits between those of Dy^{3+} and Ho^{3+}. In the same series, the *x* and *y* coordinates of F increase and indicate a stronger distortion of the M coordination polyhedron. The triangle with the three caps rotates with respect to the body of the trigonal prism in such a way that the caps come closer to an edge of the prism. All those changes along the rare-earth series nicely agree with those observed for the isostructural $Na_{3x}M_{2-x}Cl_6$ compounds.[9,10]

The variation of the sodium content as a function of temperature is illustrated for the example of Yb, Tm doped blue phosphors (Table 1, nos. 4−7). Material from the same batch was heated for 20 h to different final temperatures between 550 and 620 °C. The samples were quenched by taking them out of the furnace. Because a prolonged heat treatment did not alter the properties anymore it is assumed that the samples achieved thermodynamic equilibrium within 20 h. The 14−34° 2θ ranges of the X-ray diffraction diagrams for the different preparation temperatures are shown in Figure 5. The peak positions are almost unaffected and show only a slight increase of the lattice parameters from sample 4 to 7. But peak intensities strongly vary with temperature. The integrated intensities of the peaks with the most obvious changes are shown in the upper part of Figure 5. These variations are attributed to different cation distributions in the materials. The sodium content significantly decreases with rising firing temperature, especially between 600 and 620 °C. The composition tends toward that of the cubic $5NaF{\cdot}9MF_3$ phase[3] which corresponds to $x = 0.3125$ with respect to the $Na_{3x}M_{2-x}F_6$ formula.

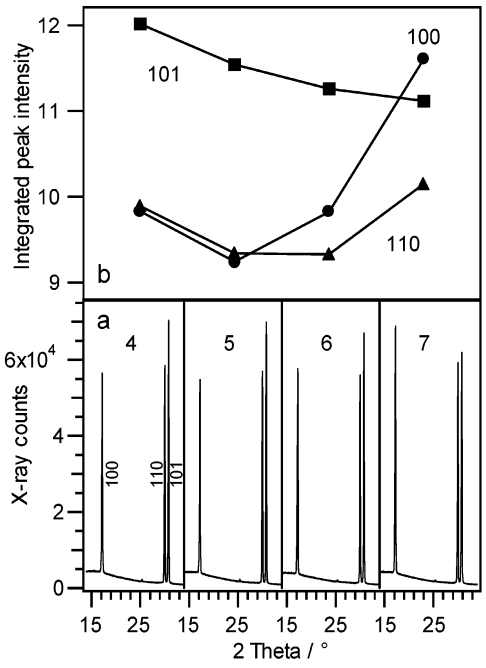

Figure 5. (a) Low-angle parts of the X-ray powder diffraction diagrams of blue phosphors for annealing temperatures of 550−620 °C. Sample numbering refers to Table 1. (b) Integrated peak intensities of the reflections.

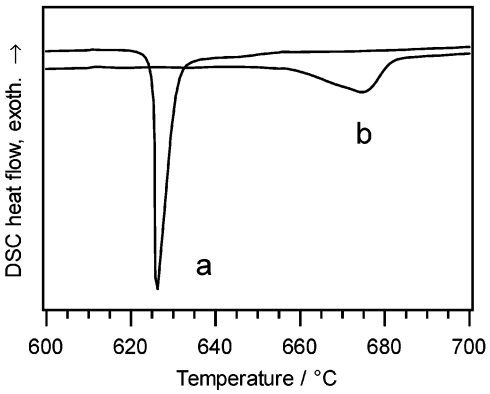

Figure 6. Differential scanning calorimetry measurement (heating curves) of a Yb, Tm doped blue phosphor, cf. Table 1, no. 6, as synthesized (a), and after the removal of excess NaF (b).

DSC Measurements. Figure 6 shows DSC measurements (heating curves) of a blue phosphor (Table 1, no. 6). Curve (a) corresponds to the "as prepared" powder containing NaF and shows the eutectic melting point

(17) Shannon, R. D. *Acta Crystallogr.* **1976**, *A32*, 751.
(18) Hughes, J. M.; Drexler, J. W. *Can. Mineral.* **1994**, *32*, 563.
(19) Kabalov, Y. K.; Sokolova, E. V.; Grigorev, A. P. *Dok. Akad. Nauk SSSR* **1993**, *330*, 713.
(20) Frank-Kamenetskaya, O. V.; Fundamenskii, V. S.; Tsytsenko, A. K.; Frank-Kamenetskii, V. A. *Kristallografiya* **1994**, *39*, 1009.
(21) Deshpande, V. P. *Acta Crystallogr.* **1961**, *14*, 794.
(22) Wickleder, M. S.; Meyer, G. *Z. Anorg. Allg. Chem.* **1998**, *624*, 1577.

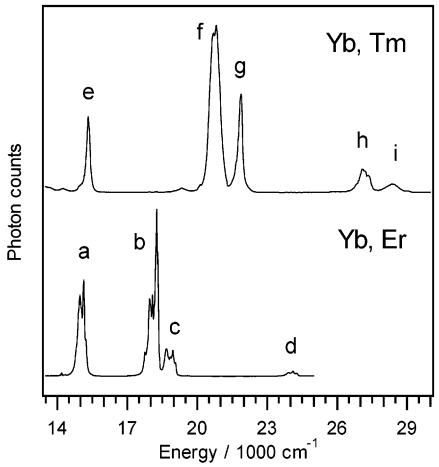

Figure 7. Room temperature UC luminescence spectra of 18% Yb, 2% Er and 25% Yb, 0.3% Tm doped phosphors prepared at 590 °C under 10 245 cm^{-1} (976 nm) Yb^{3+} excitation. The unfocused excitation power was 37 mW and 310 mW for the Yb, Er and the Yb, Tm phosphors, respectively. Labeling of the emission bands refers to Figure 8.

at 626 °C on the NaF rich side. It was reported as 638 °C for the pure Y compound.[23] Curve (b) in Figure 6 shows the hexagonal-to-cubic phase transition of the pure phosphor material after the removal of NaF by water. The maximum of the peak at 675 °C is again in good agreement with the transition in the pure Y phase at 691 °C.[23] However, the sodium content of our samples does not fit with that previously reported for the hexagonal phase.[3,23] The diagram of the pure Y compound shows a phase width of 50−53% YF_3 which corresponds to $0.5 \geq x \geq 0.456$, whereas our *x*-values range from 0.466 to 0.390 for the maximum Na content between 550 and 620 °C. Thus, the stability region of the hexagonal phase, labeled I in Figure 1 of ref 23, should be placed further to the right toward the YF_3 rich side. We can argue only on the NaF-rich border of the stability region, which is situated between about 52−58% MF_3 in the case of the Yb, Tm doped phosphor.

Upconversion Luminescence. UC luminescence spectra in the visible spectral region are shown in Figure 7 for the green and blue phosphors. The bands are labeled, and corresponding transitions are shown as arrows in the energy level diagrams of Figure 8. The most efficient excitation energy was determined as 10 245 cm^{-1} (976 nm) for both materials. It corresponds to the $^2F_{7/2} \rightarrow {}^2F_{5/2}$ absorption maximum of Yb^{3+}. This excitation energy is transferred in several steps to Er^{3+} or Tm^{3+}, respectively.

Green Phosphor. In the case of Er^{3+}, the most important excitation path is $^4I_{15/2} \rightarrow {}^4I_{11/2} \rightarrow {}^4F_{7/2}$, which requires two energy transfers from Yb^{3+}. Subsequent multi-phonon relaxation populates the emitting $^2H_{11/2}$ and $^4S_{3/2}$ states. Via further excitation and cross-relaxation processes also population of the $^2H_{9/2}$ and $^4F_{9/2}$ states is obtained. For a detailed description of the excitation mechanisms we refer to refs 1, 2, 13, and 24. The excitations lead to red (a), green (b,c), and violet (d) emissions which appear to the eye as a bright green color, cf. Figures 7 and 8. Because the various emitting

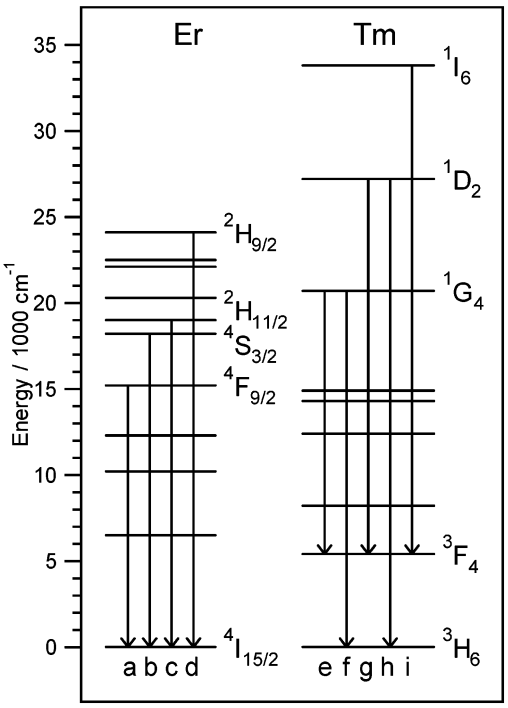

Figure 8. Energy level schemes and observed UC emission transitions of Yb, Er and Yb, Tm doped phosphors.

states are populated via different excitation paths they show distinct power dependencies. The emission intensities and the ratios of the various emissions are influenced by the doping levels, excitation power, preparation temperature, and impurities. These aspects are discussed in more detail for the blue phosphor below. For the excitation of the green phosphors in the setup shown in Figure 1, an unfocused laser beam of typically 37 mW at 10 245 cm^{-1} was used. The strongest green emission was obtained for a 18% Yb and 2% Er doped sample prepared at 590 °C. These parameters are different from those reported by Kano et al.,[11] who reported 30−40% Yb, 3−4% Er, and 630 °C as optimum parameters for their synthesis. They had to use a higher temperature to achieve a complete decomposition of their fluorinating agent $Na_2SiF_6 \rightarrow 2\ NaF + SiF_4$.

Our sample shows a 1.9 to 1 ratio of green to red photons upon unfocused excitation with 37 mW power. This ratio depends on the excitation power because the emitting states have different population mechanisms. The red emission intensity increases with respect to the green intensity with increasing Er and Yb concentration. This is due to efficient cross relaxation processes among the Er^{3+} ions at higher doping levels. We conclude that the best green UC results are obtained for Er^{3+} ions with no Er^{3+} but several Yb^{3+} neighbors for excitation energy transfer. Furthermore, a sufficient number of optically inactive Y^{3+} ions is required to avoid energy migration from the active ions to killer traps.

The detrimental effect of oxygen contamination and impurity phases on the UC efficiency is shown in Figure 9. The effect of oxygen contamination was determined for two samples, one of which was fluorinated with a HF/Ar mixture (a) during the synthesis and the other one which was treated with Ar gas (b) only. The green and the green plus red emissions of the fluorinated sample are 5.2 and 3.2 times stronger, respectively, than

(23) Thoma, R. E.; Hebert, G. M.; Insley, H.; Weaver, C. F. *Inorg. Chem.* **1963**, *2*, 1005.

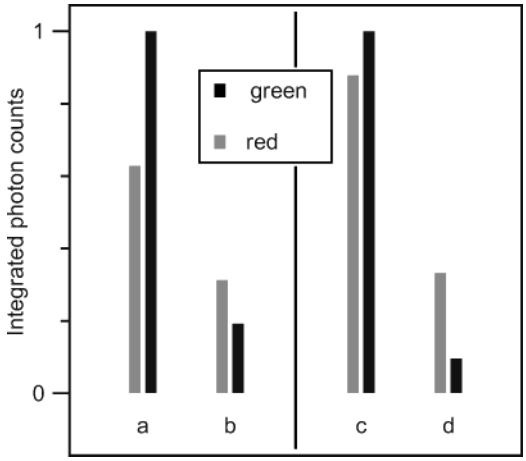

Figure 9. Integrated green ($^2H_{11/2} + {}^4S_{3/2} \rightarrow {}^4I_{15/2}$) and red ($^4F_{9/2} \rightarrow {}^4I_{15/2}$) UC photon counts of Yb, Er doped phosphors as a function of oxide contamination and crystallographic phase. Samples (a) and (b) were both prepared at 600 °C but fluorinated with HF/Ar gas or treated only with Ar gas, respectively. Samples of the hexagonal (c) and the cubic (d) phase were prepared at 650 and 750 °C, respectively.

those for sample b. Oxygen impurities increase the multi phonon relaxation rates between the metastable states with the effect of reducing the overall visible emission intensity and enhancing the red-to-green emission ratio.

The different UC efficiencies of the hexagonal and cubic sodium yttrium fluoride phase are demonstrated on the right side of Figure 9. The hexagonal phase (c) prepared at 650 °C shows a 10-times stronger green emission than the cubic phase (d) prepared at 750 °C. The green plus red emissions of the hexagonal phase are 4.4 times stronger than those for the cubic one.

Blue Phosphor. The excitation paths in the blue Yb, Tm phosphor are more complex than those in the green Yb, Er phosphor. Three and four energy transfer steps from Yb^{3+} $^2F_{5/2}$ to Tm^{3+} are required to populate $^1G_4$ and $^1D_2$, respectively. We refer to refs 1, 2, 24, and 25 for a detailed discussion. As shown in Figure 8, the visible luminescence originates from two states: $^1G_4 \rightarrow {}^3F_4$ results in a red (e) emission and $^1G_4 \rightarrow {}^3H_6$ results in a blue (f) emission. The $^1D_2 \rightarrow {}^3F_4$ transition gives rise to an additional blue emission (g). Furthermore, substantial ultraviolet emissions occur due to the $^1D_2 \rightarrow {}^3H_6$ (h) and the $^1I_6 \rightarrow {}^3F_4$ (i) transitions, especially at high excitation powers. Because the Tm excitation involves higher order processes compared to the predominantly two step excitation of Er, higher excitation power is required to obtain a comparable visible emission intensity. The emission experiments shown in Figures 7, 10, and 11 were excited with typically 310 mW unfocused laser power at 10 245 cm^{-1}.

The blue emission intensities of Yb, Tm doped phosphors are shown in Figure 10 as a function of the preparation temperature. The samples correspond to Table 1, nos. 4−7. They were synthesized under identical conditions except for the temperature in the final annealing step. The emission intensities show a clear maximum for the samples prepared between 580 and 600 °C. As is obvious from Figure 5, all samples consist

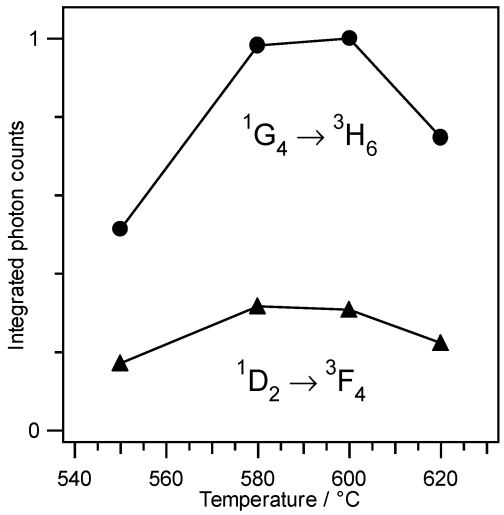

Figure 10. Integrated blue UC photon counts of Yb, Tm doped phosphors as a function of the preparation temperature, cf. Table 1, nos. 4−7.

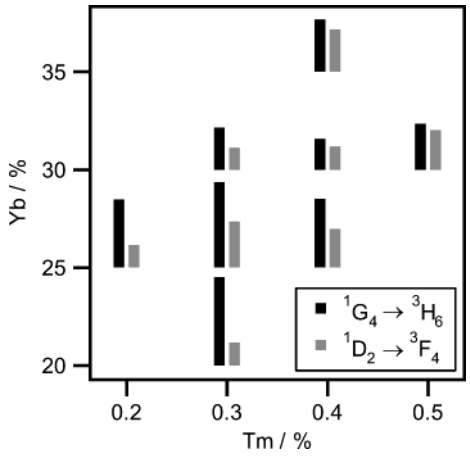

Figure 11. Integrated blue UC photon counts as a function of the Yb and Tm doping levels.

of the hexagonal phase and show comparable crystallinity, but they differ with respect to their sodium content, and the phosphor particle size slightly increases from 550 to 620 °C. The optimum preparation temperature of 590 ± 10 °C is distinctly lower than those reported in previous work.[11,12] It is situated about 35 K lower than the eutecticum. Above 600 °C the cation sublattices change significantly, which points toward an enhanced ion mobility in the solid phase close to the eutectic temperature. With increasing temperature the sodium content in the hexagonal phase decreases and tends toward the composition of the cubic phase which has a substantially lower UC efficiency.

The effect of the dopant concentration on the UC emission intensity is demonstrated in Figure 11. Because the blue emissions originate from different states and population mechanisms, they show distinct dopant dependencies. The strongest $^1G_4$ emission is observed for 20% Yb and 0.3% Tm doping. The strongest $^1D_2$ emission occurs for 25% Yb and 0.3% Tm, but it gains relative importance toward higher doping levels. Because the $^1D_2$ population is of higher order than the $^1G_4$ excitation, it is favored by higher Tm and Yb concentrations. If both blue emissions are added together, the optimum doping levels are 25% Yb and 0.3% Tm.

(24) Gamelin, D. R.; Güdel, H. U. *Top. Curr. Chem.* **2001**, *214*, 1.
(25) Antipenko, B. M.; Dumbravyanu, R. V.; Perlin, E.; Raba, O. B.; Sukhareva, L. K. *Opt. Spectrosc.* (USSR) **1985**, *59*, 377.

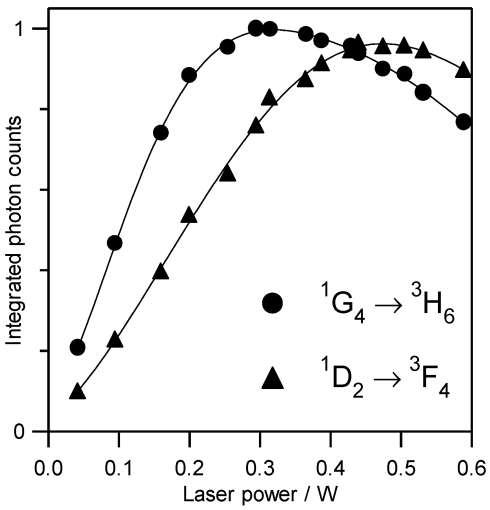

Figure 12. Integrated blue UC photon counts of a Yb, Tm doped phosphor (cf. Table 1, no. 6) as a function of focused (f = 14.5 mm) excitation power at 10 245 cm^{-1}. The lines are drawn as guides to the eye.

The various UC emission bands show different power dependencies due to their different excitation mechanisms. In the low power regime, the blue UC emissions show slopes between 3 and 3.7 in a double logarithmic representation. This is in agreement with 3 and 4 photon excitation processes for $^1G_4$ and $^1D_2$ in Tm^{3+}, respectively. The blue UC intensities in the high power regime are shown in Figure 12 on a linear scale. In contrast to previous Figures, the results shown in Figures 12 and 13 were obtained with the excitation laser beam focused by a diffraction limited lens multiplet (f = 14.5 mm, NA = 0.276, spot size = 2.75 μm, Melles Griot). Under these high excitation density conditions, the power dependencies do not follow simple power laws anymore, which are used for the characterization of the mechanisms in the low power regime. The $^1G_4$ and $^1D_2$ emissions saturate at 300 mW and 450 mW, respectively, and then decline for increasing power because the sample is increasingly warmed by the rising number of nonradiative relaxation processes.

The phosphor materials were investigated for degradation under high power laser excitation. The UC intensity of the blue $^1G_4 \rightarrow {}^3F_4$ transition is shown in Figure 13 for 456 mW focused excitation at 10 245 cm^{-1}. The sample was repetitively illuminated for 40 s and the beam was blocked for 20 s in between. After an initial spike, the emission intensity decreases to a stable value determined by the steady state of the sample in the focused laser beam. The emission intensity reaches the same level after each cycle, and no degradation was observed after 2 h. This behavior stands in striking contrast to that of a commercial sodium yttrium fluoride UC phosphor obtained from Sarnoff Research Laboratories, Princeton, NJ, which was used as a reference. For the same excitation conditions this material degrades significantly and irreversibly within the first five minutes. The decrease in the light output was accompanied by chemical decomposition, the products of which produced a hole in the glass wall of the sample tube. Presumably, the glass was etched by HF gas. Its origin might be the thermal decomposition of NH_4F or other hydrofluorides or its liberation from enclosures of the phosphor powder dating back to a hydrothermal synthesis. The stability of our material at the saturation level of the excitation and above demonstrates its high application potential for lighting or display devices.

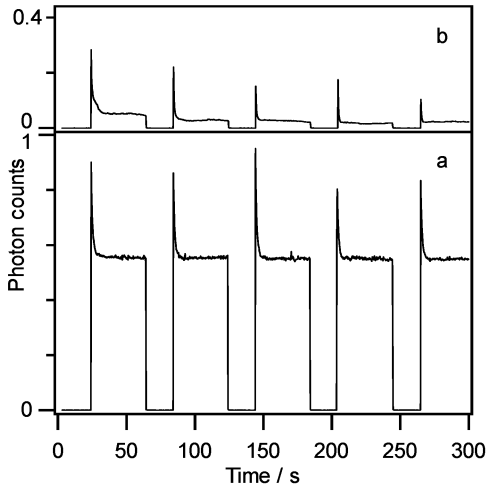

Figure 13. Phosphor stability under high-power laser excitation. The blue $^1D_2 \rightarrow {}^3F_4$ emission of sample 6, Table 1, (a) and of a commercial Yb, Tm doped sodium yttrium fluoride phosphor (b) was monitored as a function of time under focused (f = 14.5 mm) 456 mW excitation at 10 245 cm^{-1} (cf. Figure 12).

In summary, we report a new, reproducible synthesis method for highly efficient, chemically and physically stable UC phosphor materials of the pure hexagonal sodium yttrium fluoride phase. A new structural model was developed which accounts for the cation distribution and the nonstoichiometry of this phase. The phase purity, sodium content, preparation temperature, doping levels, and excitation power were optimized with respect to the UC emission intensity of the green and blue phosphors.

Acknowledgment. We thank B. Frey and U. Kindler for valuable support in the analytical measurements and the construction of the HF gas handling system, respectively. Financial support by the Swiss National Science foundation is gratefully acknowledged.

CM031124O